Biolighted Nanotorch Capable of Systemic Self-Delivery and Diagnostic Imaging

Ajay Singh,[†,∥,∞] Young Hun Seo,[†,‡,∥] Chang-Keun Lim,[†,∞] Joonseok Koh,[§] Woo-Dong Jang,[‡] Ick Chan Kwon,[†] and Sehoon Kim*[,†]

[†]Center for Theragnosis, Korea Institute of Science and Technology (KIST), 39-1, Hawolgok-dong, Sungbuk-gu, Seoul 136-791, Korea, [‡]Department of Chemistry Yonsei University, 50 Yonsei-ro, Seodaemungu, Seoul 120-749, Korea, and [§]Department of Organic and Nano System Engineering, Konkuk University, Seoul 143-701, Korea. [∥]A.S. and Y.H.S. contributed equally to this work. [∞]Present address: Institute for Lasers, Photonics and Biophotonics, Department of Chemistry, State University of New York, Buffalo, NY 14260, USA.

ABSTRACT Sensitive imaging of inflammation with a background-free chemiluminescence (CL) signal has great potential as a clinically relevant way of early diagnosis for various inflammatory diseases. However, to date, its feasibility has been limitedly demonstrated *in vivo* with locally induced inflammation models by *in situ* injection of CL probes. To enable systemic disease targeting and imaging by intravenous administration of CL probes, hurdles need to be overcome such as weak CL emission, short glowing duration, or inability of long blood circulation. Here, we report a CL nanoprobe (BioNT) that surmounted such limitations to perform precise identification of inflammation by systemic self-delivery to the pathological tissues. This BioNT probe was engineered by physical nanointegration of multiple kinds of functional molecules into the ultrafine nanoreactor structure (~15 nm in size) that combines solid-state fluorescence-induced enhanced peroxalate CL and built-in machinery to control the intraparticle kinetics of CL reaction. Upon intravenous injection into a normal mouse, BioNT showed facile blood circulation and generated a self-lighted strong CL torchlight throughout the whole body owing to the tiny colloidal structure with an antifouling surface as well as high CL sensitivity toward endogenous biological hydrogen peroxide (H_2O_2). In mouse models of local and systemic inflammations, blood-injected BioNT visualized precise locations of inflamed tissues with dual selectivity (selective probe accumulation and selective CL reaction with H_2O_2 overproduced by inflammation). Even a tumor model that demands a long blood circulation time for targeting (>3 h) could be accurately identified by persistent signaling from the kinetics-tailored BioNT with a 65-fold slowed CL decay rate. We also show that BioNT exhibits no apparent toxicity, thus holding potential for high-contrast diagnostic imaging.

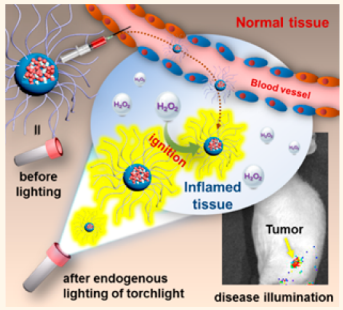

KEYWORDS: chemiluminescence · diagnosis · *in vivo* imaging · nanoprobes · systemic delivery

Chemiluminescence (CL) is the light emission produced by a specific chemical reaction, whose intensity is proportional to the concentration of reactive analytes, being useful for a wide range of analytical applications.[1] Unlike photoluminescence (PL) by light excitation, CL measurements do not involve sources of background noise such as autofluorescence from the biological specimen or stray excitation light, offering extraordinary sensitivity in autofluorescence-rich *in vivo* media.[2,3] Bioluminescence is a type of CL catalyzed by an enzyme and has been well exploited for *in vivo* imaging.[3] However, it demands genetic expression of the exogenous enzyme and coadministration of the luminescent substrate, being incompatible with clinical purposes. In recent years, nonenzymatic peroxalate-based CL (POCL) has been applied to *in vivo* imaging of local inflammation.[4−6] Hydrogen peroxide (H_2O_2), abnormally overproduced in the progress of inflammatory diseases,[7] triggers a POCL reaction, i.e., oxidation of peroxalates to form 1,2-dioxetanedione that can transfer its high energy to nearby fluorescent molecules to emit CL. POCL nanoprobes (nanoscale reactors loaded with peroxalates and dyes) showed high sensitivity and selectivity toward H_2O_2, holding potential for early diagnosis of inflammation. This advantageous feature has been conceptually demonstrated by direct local injection of POCL nanoprobes into the inflamed tissues; however it remains a challenge to make them operable by systemic delivery, which would allow for more advanced diagnostic

* Address correspondence to sehoonkim@kist.re.kr.

Received for review June 4, 2015 and accepted August 28, 2015.

Published online August 28, 2015
10.1021/acsnano.5b03377

imaging by sensitively discovering and locating inflammations in the body with background-free CL signals.

As demonstrated in our previous report, colloidal POCL nanoprobes filled with a highly reactive peroxalate (bis[3,4,6-trichloro-2-(pentyloxycarbonyl)phenyl]oxalate, CPPO) and a typical NIR-emissive cyanine dye (Cy5) could detect *in vivo* H_2O_2 as low as $\sim 5 \times 10^{-8}$ M.[5] A simple way to further enhancement is to utilize a special dye that emits solid-state fluorescence (SSF) without typical self-quenching of fluorescence.[8−11] By concentrating the POCL nanoreactor with an SSF dye in place of a dilute Cy5 dopant, the CL intensity could be simply enhanced by 1 order of magnitude.[6] An intriguing aspect of the SSF-induced enhanced POCL (SSF-CL) is that the achieved detection limit is far below the normal physiological level of H_2O_2 (10^{-7} M).[12] The resulting ultrahigh sensitivity may render the following scenario plausible: (1) Upon systemic administration of the nanoprobes, the SSF-CL reaction can be triggered even by the normal *in vivo* level of H_2O_2 to emit an endogenously lighted luminescence glow. (2) If the lighted nanoprobes are capable of long blood circulation, they can illuminate the whole body to produce a self-glowing living body and then accumulate in pathological tissues where the CL intensity reflects the level of H_2O_2 abnormally overproduced by inflammation.

In the present study, we demonstrate that such a scenario is feasible with an ultrafine POCL nanoreactor (~15 nm in size) that is capable of strong SSF-CL emission as well as self-delivery to the diseased sites (delivery by itself through passive accumulation based on the enhanced permeability and retention (EPR) effect[13]). This nanoreactor is hereafter called "biolighted luminescent nanotorch (BioNT)" because SSF-CL is lighted and sustained by the reaction between nanoscopically confined fuels (peroxalates) and endogenous biological H_2O_2 and then extinguished after complete fuel consumption, as is torchlight. In order for BioNT to well reflect the diagnostic H_2O_2 level, its CL torchlight needs to be persistent even after blood circulation and disease accumulation. To control the duration of torchlight to be long enough for imaging a disease that demands a long blood circulation for systemic targeting, we devised a simple way of tailoring the luminescence kinetics by loading the nanotorch with antioxidants. Here we present a proof-of-concept study on the self-delivery and luminescence kinetics control of blood-circulating BioNT and its on-demand uses for diagnostic imaging of diseases by systemic injection.

RESULTS AND DISCUSSION

BioNT and its constituents are sketched in Figure 1a. As an emitting component for POCL, we employed an anthracene-cored hydrophobic dye (BDSA; see Scheme S1 in the Supporting Information) whose chromophoric unit has been reported to show strong

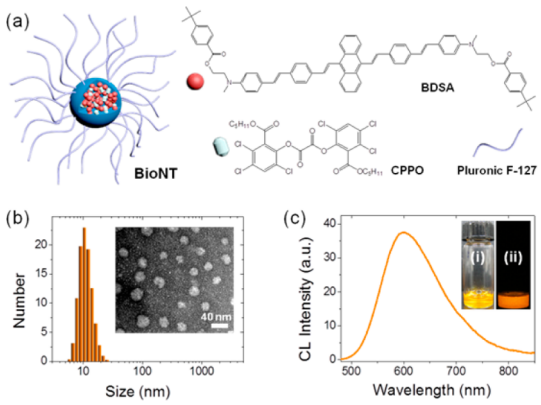

Figure 1. (a) Schematic representation of BioNT. (b) Number-averaged hydrodynamic size distribution and TEM image (inset) of BioNT. (c) CL spectrum of water-dispersed BioNT, taken at 10 s after addition of H_2O_2 (0.17 M). The inset shows photographs of the generated CL under room light (i) and in the dark (ii).

reddish SSF in the nanoaggregated forms.[14−16] To construct SSF-incorporated POCL nanoreactors, an aqueous dispersion of dye/peroxalate coaggregates was formulated by excess loading of BDSA and CPPO within micellar nanoparticles of a polymeric surfactant, Pluronic F-127. The fabrication was done in two steps: (1) homogeneous mixing of Pluronic F-127, CPPO, and BDSA in a methylene chloride solution and (2) subsequent addition of water to the dried ternary mixture to disperse amphiphilically self-assembled nanoparticles where the hydrophobic molecules (BDSA and CPPO) are coaggregated in the core of the micellar nanoparticles and the surface is passivated with the hydrophilic/antifouling block of Pluronic F-127. From the TEM and dynamic light-scattering (DLS) measurements, the average diameter and the number-weighted hydrodynamic size of BioNT were estimated as 15.8 ± 4.8 and 15.4 ± 0.5 nm (Figure 1b), respectively, manifesting that the colloidal size was suitably engineered to be small enough for long systemic circulation.[13]

Upon photoexcitation at 430 nm, BioNT exhibited intense reddish PL ($\lambda_{max.PL}$ = 584 nm, Φ_f = 0.41; see Figure S1 in the Supporting Information), which is typical of the SSF of BDSA. The spectrum showed a slight hypsochromic shift compared to the F-127 nanoparticles of BDSA-only aggregates ($\lambda_{max.PL}$ = 607 nm, Φ_f = 0.44), indicating that the BDSA molecules are loosely packed in the particle matrix due to the coaggregation with CPPO.[6] Typically, the emission spectrum is broad and, thus, significantly covers the tissue-penetrating near-infrared (NIR) region (>650 nm), being advantageous for *in vivo* imaging. Upon addition of H_2O_2 to the BioNT dispersion, reddish luminescence was generated with the characteristic SSF spectrum of BDSA (Figure 1c). The CL output from BioNT was so strong as to be seen vividly by the naked eye under room light (the inset of Figure 1c), suggesting that the

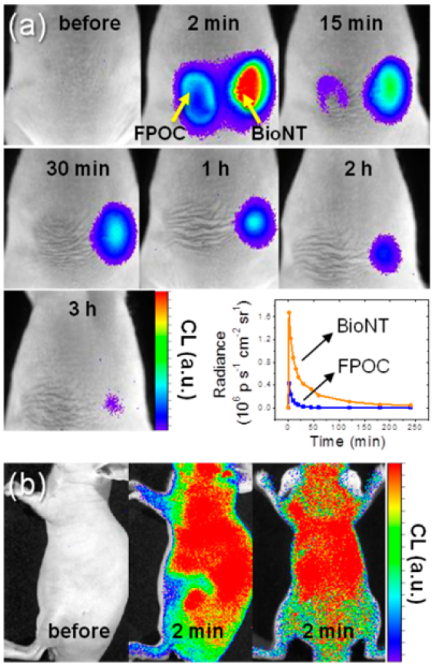

Figure 2. Biolighted luminescent torchlight in normal conditions *in vivo*. (a) Images and intensity profiles of endogenously generated CL from BioNT and a Cy5-doped POCL nanoprobe (FPOC), both of which were injected subcutaneously into the dorsal side of a normal mouse as indicated (n = 4). (b) CL images (side and dorsal views) of a normal mouse before and 2 min after the tail vein injection of BioNT (n = 4).

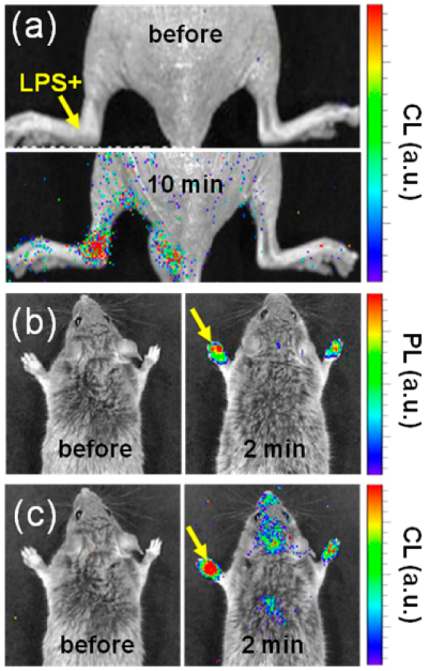

Figure 3. Imaging of localized and systemic arthritis with intravenously injected BioNT (n = 4). (a) CL images of localized acute arthritis induced by intra-articularly preinjected LPS 48 h prior to imaging. (b, c) Systemic inflammation model of rheumatoid arthritis (RA) imaged with PL (b) and CL (c) signals. LPS-injected ankle (a) and more inflamed foot (b, c) are indicated with arrows.

aggregated BDSA and CPPO are a good pair for the POCL reaction.

The luminescence characteristics of SSF-based BioNT were evaluated in comparison to a typical dye (Cy5)-doped POCL nanoprobe (FPOC).[5] Upon subcutaneous injection to a normal mouse, both BioNT and FPOC displayed biolighted CL (lighted by endogenous H_2O_2 *in vivo*) whose intensity decayed with time (Figure 2a). When H_2O_2-scavenging glutathione was coinjected with BioNT, the CL intensity was reduced to a notable extent (see Figure S2 in the Supporting Information), supporting that the generated POCL is a true consequence of biological H_2O_2. The total signal output of BioNT over time is 11-fold intensified over that of FPOC, confirming that the SSF-based nanotorch can be lighted and emit enhanced luminescence even by the normal *in vivo* level of H_2O_2. More importantly, immediately after intravenous injection of BioNT into a normal mouse, a bright CL glow was seen throughout the whole body with no significant localization (Figure 2b), implying that it can circulate well along the bloodstream due to the small colloidal size and the antifouling surface coat. The bright CL was observed only from the nanoreactor sample containing both BDSA and CPPO (see Figure S3 in the Supporting Information), supporting that the torchlight is SSF-CL generated by the POCL reaction among BDSA, CPPO, and endogenous H_2O_2. All these observations, along with the colloidal and optical stabilities under physiological conditions (see Figure S4 in the Supporting Information), confirm that BioNT satisfies the suggested requirements for the success of systemically targeted CL imaging, *i.e.*, ultrahigh H_2O_2 sensitivity and facile blood circulation.

H_2O_2-overproducing inflammatory diseases such as atherosclerosis, cancer, arthritis, or ischemia, are known to develop defective leaky vasculature.[17] Such pathological tissues can be passively targeted with nanomaterials capable of long blood circulation.[18,19] Indeed, blood-circulating BioNT showed fast self-delivery to the inflamed tissues upon intravenous injection. As seen by CL imaging, the lipopolysaccharide (LPS)-induced local inflammation in the mouse ankle joint was readily targeted and visualized within 10 min by the tail vein injection of BioNT (Figure 3a). The inflamed-to-normal contrast ratio of CL (~12) was 2-fold higher than that of PL (see Figure S5 in the Supporting Information), validating the merit of autofluorescence-free CL modality.

Systemic self-delivery of the H_2O_2-imaging BioNT would provide an opportunity for the noninvasive detection and diagnosis of systemic inflammatory disorders in the body. For example, rheumatoid arthritis (RA) that is a chronic autoimmune disorder and occurs systemically could be successfully located and visualized in a mouse model with diagnostic CL signals from the intravenously injected BioNT. In visual examination of the RA model, only the left forepaw seemed

inflamed with apparent arthritic symptoms of redness and swelling. Upon intravenous injection of BioNT, however, its PL signals were observed in both left and right forepaws as early as 2 min postinjection and shown to accumulate gradually with time (Figure 3b). The PL signal accumulation is attributed to the population enrichment of BioNT by self-delivery, suggesting that both forepaws are in the arthritic condition with leaky blood vessels. The left forepaw that was apparently more inflamed showed a higher PL intensity than the right that presented no apparent sign of inflammation ($I_{PL,left}/I_{PL,right} \sim 1.2$ at 2 min). This manifests that a larger number of nanoprobes accumulated in the left due to the more developed pathological condition. Importantly, such a diagnostic signal contrast was more enhanced by CL modality. As shown in Figure 3c, CL imaging of the same mouse showed a more clear-cut imaging contrast between the developed and early inflammations ($I_{CL,left}/I_{CL,right} \sim 2.1$ at 2 min). This validates that the CL intensity reflects not only the self-delivered nanoprobe population but also molecular information on the overproduced inflammatory H_2O_2 level in the delivered tissue. The combined performance of systemic self-delivery and H_2O_2-responsive molecular imaging well represents the potential merit of SSF-enhanced luminescent BioNT for the diagnostic functional imaging.

In the above demonstration, systemically injected BioNT was rapidly self-delivered to the arthritic tissues long before extinction of the POCL torchlight, which rendered diagnostic imaging of the inflammatory H_2O_2 successful. In general, however, passive disease targeting demands prolonged blood circulation that could be longer than the CL lifetime of BioNT. For instance, it was found that tumor targeting by intravenously injected BioNT took at least 3 h; therefore, the CPPO fuel was almost consumed and the inflammatory H_2O_2 level of the tumor was hard to image with the expiring CL torchlight (see Figure S6 in the Supporting Information). Such a limitation could be overcome by prolonging the glowing duration of the short-lived POCL emission. To tailor the decay kinetics, BioNT was further loaded with a hydrophobic derivative of ascorbic acid (ascobyl palmitate) that is an antioxidant known to break oxidative H_2O_2 into H_2O (Figure 4a and see Figure S7 in the Supporting Information). To see the antioxidant effect on the kinetics, BioNT particles with and without coembedded ascorbyl palmitate (AP) were subcutaneously injected, and their biolighted CL signals were compared *in vivo* with time. As shown in Figure 4b, the luminescence from antioxidant-free pristine BioNT was initially brighter but faded faster than that from antioxidant-loaded BioNT (BioNT+AP). These *in vivo* luminescing behaviors were well expressed by following a simple pseudo-first-order kinetic profile[5,6] (Figure 4c). BioNT+AP presented the rise and decay kinetic rates ($k_r = 7.8 \times 10^{-3}\ s^{-1}$ and

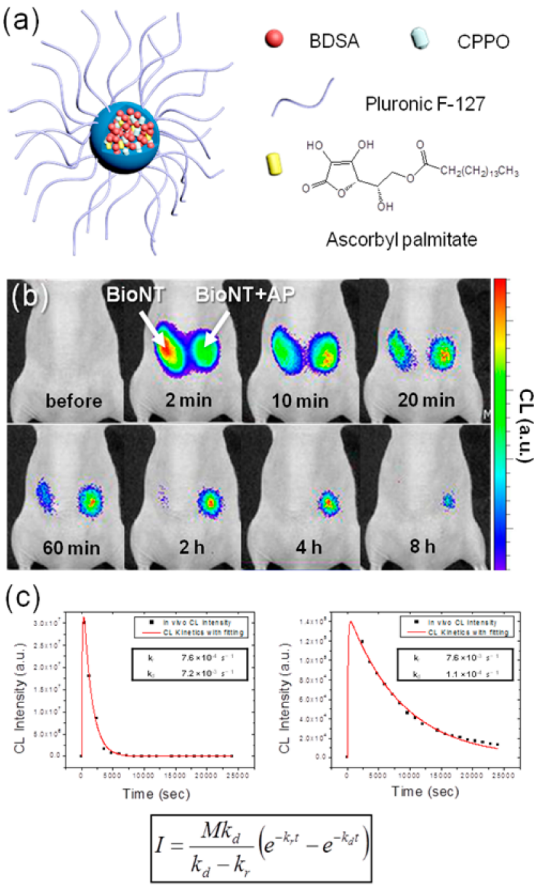

Figure 4. (a) Schematic representation of ascorbyl palmitate (AP) coembedded BioNT (BioNT+AP). (b) Temporal intensity traces of endogenously generated CL from antioxidant-free BioNT and antioxidant-loaded one (BioNT+AP), both of which were injected subcutaneously into the dorsal side of a normal mouse as indicated ($n = 4$). (c) *In vivo* CL kinetic profiles of antioxidant-free BioNT (left) and BioNT+AP (right). The CL intensities were taken from the CL images in (b). The kinetic parameters were determined with nonlinear fitting according to the given equation, where I is the CL intensity. k_r and k_d are the rate constants for rising and decay, respectively.

$k_d = 1.1 \times 10^{-4}\ s^{-1}$) that were 65-fold slowed compared to those of the antioxidant-free one ($k_r = 7.6 \times 10^{-4}\ s^{-1}$ and $k_d = 7.2 \times 10^{-3}\ s^{-1}$). It is speculated that the given antioxidizing intraparticle environment might reduce the input concentration of biological H_2O_2, and thus, the limited oxidant concentration could slow down the consumption of CPPO. As a result, antioxidant-loaded BioNT sustained imagible CL signaling *in vivo* even at 8 h postinjection, as opposed to the short-lived antioxidant-free probe signal that became negligible as early as 2 h after injection (Figure 4b). In spite of the big difference in CL kinetics, total CL outputs over time from both BioNTs were found to be similar when integrated for 3 h *in vitro* at the H_2O_2 concentration close to the normal *in vivo* level (5×10^{-7} M). Compared to antioxidant-free BioNT, BioNT+AP showed only a slight reduction (~14%) in the total CL output (see Figure S8 in the Supporting Information), suggesting

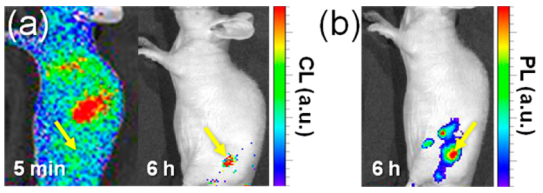

Figure 5. (a) CL images showing the temporal signal distribution of intravenously injected BioNT+AP into a mouse bearing a small SCC7 tumor (~45 mm^3), taken at the indicated time points after tail vein injection (n = 4). (b) PL image of the same mouse in (a), taken at 6 h postinjection (n = 4). Yellow arrows indicate the tumor location.

that antioxidant coencapsulation minimally influences the time-integrated CL sensitivity toward H_2O_2.

With similar colloidal sizes and stabilities (see Figure S4 in the Supporting Information), the intravenously injected BioNT and BioNT+AP probes displayed almost identical behaviors of long-circulating tumor targeting, as seen by PL imaging (see Figures S6 and S9 in the Supporting Information). However, CL imaging presented a significant alteration by the antioxidant-effected kinetics modulation (Figure 5a and see Figure S6 in the Supporting Information). After accumulation of the probes, the tumor was hardly imaged with the short-lived CL from antioxidant-free pristine BioNT, whereas in the case of BioNT+AP the H_2O_2-overproducing tumoral condition was clearly visualized at 6 h postinjection with the still glowing torchlight. Importantly, it is noted that PL imaging yielded a number of off-target signals from other parts of the body (e.g., lymph nodes) due to less disease-specific tissue accumulation of the probes (Figure 5b). Such nonspecific false signals are typical of a PL modality that merely depends on the biodistribution of PL probes, which compromises the accuracy of image-based diagnosis. In sharp contrast, CL imaging at the same time point visualized only the location of an invisible early stage tumor smaller than 50 mm^3 exclusively because the tumoral tissue has a higher level of H_2O_2 than other nonspecifically accumulated parts of the body (Figure 5a). This result demonstrates the advantage of the long-lasting luminescent torchlight of BioNT that allows for precise diagnostic signaling with dual selectivity, *i.e.*, selective probe enrichment in the pathological tissue by self-delivery and selective generation of prolonged SSF-CL by the pathological tissue-specific level of H_2O_2. Favorable biodistribution and minimal impacts on the animal viability with no significant sign of toxicity further validate the *in vivo* utility of BioNT+AP as a systemic probe for diagnostic molecular imaging (see Figures S10−12 in the Supporting Information).

CONCLUSION

In summary, we have developed a biologically light-able CL nanotorch (BioNT) that is useful for systemically targeted imaging and precise identification of inflamed tissues *in vivo*. The construction of BioNT is based on the physical integration of reactants into a self-assembled nanoreactor system wherein the SSF-CL reaction is triggered even by the normal *in vivo* level of H_2O_2. It has been demonstrated that the intensity of the concomitantly generated CL torchlight well reflected the inflammatory H_2O_2 level in the background-rich biological tissues. Besides sensitive visualization of H_2O_2, BioNT was shown to be capable of systemic self-delivery to the pathological tissues and elaborate control of luminescence kinetics. The combined merits allowed for systemically targeted diagnostic imaging with selectively enhanced dual contrasts between the normal and inflamed tissues in terms of probe population and H_2O_2 concentration. Taking into account low *in vivo* toxicity shown in our experiments, we believe that our BioNT probe holds great potential for diagnostic biomedical uses.

EXPERIMENTAL SECTION

Materials and Instrumentation. All chemical reagents were purchased from Aldrich and TCI and used as received. Chemical structures were identified by ^{1}H and ^{13}C NMR, elemental analysis, and mass spectroscopy (Varian unity plus 300). Absorption spectra were measured on a UV−vis spectrometer (Agilent 8453). Chemi- and photoluminescence spectra were recorded on an F-7000 fluorescence spectrophotometer (Hitachi, wavelength calibrated for excitation and emission). The nanoparticle size distribution was determined by a dynamic light scattering (DLS) method using a particle sizer (90Plus, Brookhaven Instruments Corp.) at 25 °C. Transmission electron microscopic (TEM) image of negatively stained particles (with 2 wt % uranyl acetate) was obtained with a CM30 electron microscope (FEI/Philips) operated at 200 kV.

9,10-Bis[4′-[4″-[*N*-methyl-*N*-(2-[4-*tert*-butylbenzoyloxy]ethyl)amino]-styryl]styryl]anthracene (BDSA). To a solution of **2**[13] (0.2 g, 0.27 mmol; Scheme S1) in NMP (5 mL) and triethylamine (1 mL) in argon atmosphere was slowly added *tert*-butyl benzoyl chloride (0.268 g, 1.36 mmol) in an ice bath, and the reaction mixture was stirred overnight at room temperature. After completion of reaction, the reaction mixture was poured into brine and extracted with dichloromethane two times. The collected organic phase was dried over $MgSO_4$, and the solvent was evaporated at reduced pressure. The residue was purified by using column chromatography on a silica gel. The eluting impurities were removed using THF/*n*-hexane (1/5 by volume), and then the product was collected by eluting with dichloromethane. Yield: 0.192 g (67%). ^{1}H NMR (400 MHz, $CDCl_3$, ppm): *d* 8.44 (dd, 4H, *J* = 3.3, 6.6 Hz); 8.04 (d, 4H, *J* = 8.1 Hz); 7.94 (d, 2H, *J* = 16.5 Hz); 7.71 (d, 4H, *J* = 8.1 Hz); 7.60 (d, 4H, *J* = 8.1 Hz); 7.52−7.44 (m, 14H); 7.16 (d, 2H, *J* = 16.2 Hz); 7.01 (d, 2H, *J* = 16.2 Hz); 6.97 (d, 2H, *J* = 16.5 Hz); 6.83 (d, 4H, *J* = 8.7 Hz); 4.52 (t, 4H, *J* = 5.7 Hz); 3.82 (t,4H, *J* = 5.7 Hz); 3.10 (s, 6H), 1.35 (s, 18H). ^{13}C NMR (150 MHz, DMSO-d_6, ppm): 166.78, 156.46, 149.35, 137.57, 136.76, 136.16, 129.62, 129.34, 128.78, 127.12, 127.91, 126.78, 126.35, 126.16, 125.42, 124.91, 124.53, 112.37, 111.72, 61.45, 58.16, 39.46, 34.68, 30.31. MS (MALDI) *m/z*: $[M + H]^+$ calcd for $C_{74}H_{72}N_2O_4$ 1052.55, found 1052.16. Anal. Calcd for $C_{74}H_{72}N_2O_4$: C, 84.38; H, 6.89; N, 2.66; O, 6.08. Found: C, 84.45; H, 6.96; N, 2.71; O, 6.16.

Preparation of BDSA Nanoaggregates. A polymeric dispersion of BDSA nanoaggregates was prepared with Pluronic F-127 for the

study of SSF behavior. The mixture of BDSA (1 mg) and Pluronic F-127 (20 mg, Aldrich) was homogeneously dissolved in THF solution (0.2 mL). The solvent was evaporated by air drying. Milli-Q water (1 mL) was added to the dried mixture-coated vial, and the vial was then vigorously shaken to produce a clear dispersion.

Preparation of BioNT Particles. BDSA (1 mg) was homogeneously mixed with Pluronic F-127 (20 mg, Aldrich) and bis-[3,4,6-trichloro-2-(pentyloxycarbonyl)phenyl] oxalate (CPPO, 1 mg, TCI) in THF (0.6 mL). After the solvent was evaporated by air flow, the dried mixture was mixed with Milli-Q water (1 mL) and then vigorously shaken to afford an aqueous dispersion of self-assembled BioNT. An antioxidant-loaded BioNT(BioNT+AP) was prepared by following the same procedure with ascorbyl palmitate (0.02 mg) added to the above mixture.

Animal Experiments. The animal studies have been approved by the animal care and use committee of Korea Institute of Science and Technology, and all handling of mice was performed in accordance with the institutional regulations. Disease models were prepared using BALB/c nude mice (male, 5 weeks of age, Orient Bio Inc. Korea; tumor and LPS-induced inflammation) and DBA/1J mice (male, 5 weeks of age, Jungang Lab Animal, Seoul, Korea; rheumatoid arthritis) by anaesthetizing with intraperitoneal injection of 0.5% pentobarbital sodium (0.01 mL/g). Tumor xenografts and LPS-induced inflammation were created by subcutaneous injection of a suspension of 1×10^7 SCC7 cells in RPMI1640 cell culture medium and by intra-articular injection of lipopolysaccharide (20 μL, 2 mg/mL in PBS), respectively. Rheumatoid arthritis (RA) was induced by immunization through intradermal injection of the emulsion (50 μL) of bovine type-II collagen into the tail.[20] *In vivo* imaging experiments were done with anaesthetized mice at certain time points after disease model preparation (2 weeks for tumor with a size of ~45 mm^3; 48 h for LPS-induced inflammation and 6 weeks for rheumatoid arthritis) by tail vein injection of the BioNT particles (200 μL). *In vivo* imaging was done with an IVIS Spectrum imaging system (Caliper, USA).

Conflict of Interest: The authors declare no competing financial interest.

Supporting Information Available: The Supporting Information is available free of charge on the ACS Publications website at DOI: 10.1021/acsnano.5b03377.

Supplemental scheme and figures (PDF)

Acknowledgment. This work was supported by grants from the National Research Foundation of Korea (no. H-GUARD_2014-M3A6B2060522 and 2014M3C1A3054141) and the Intramural Research Program of KIST.

REFERENCES AND NOTES

1. Kricka, L. J. Clinical Applications of Chemiluminescence. *Anal. Chim. Acta* **2003**, *500*, 279–286.
2. Lee, J.-J.; White, A. G.; Rice, D. R.; Smith, B. D. *In Vivo* Imaging Using Polymeric Nanoparticles Stained with Near-Infrared Chemiluminescent and Fluorescent Squaraine Catenane Endoperoxide. *Chem. Commun.* **2013**, *49*, 3016–3018.
3. Saito, K.; Chang, Y.-F.; Horikawa, K.; Hatsugai, N.; Higuchi, Y.; Hashida, M.; Yoshida, Y.; Matsuda, T.; Arai, Y.; Nagai, T. Luminescent Proteins for High-Speed Single-Cell and Whole-Body Imaging. *Nat. Commun.* **2012**, *3*, 1262.
4. Lee, D.; Khaja, S.; Velasquez-Castano, J. C.; Dasari, M.; Sun, C.; Petros, J.; Taylor, W. R.; Murthy, N. *In Vivo* Imaging of Hydrogen Peroxide with Chemiluminescent Nanoparticles. *Nat. Mater.* **2007**, *6*, 765–769.
5. Lim, C.-K.; Lee, Y.-D.; Na, J.; Oh, J. M.; Her, S.; Kim, K.; Choi, K.; Kim, S.; Kwon, I. C. Chemiluminescence-Generating Nanoreactor Formulation for Near-Infrared Imaging of Hydrogen Peroxide and Glucose Level *In Vivo*. *Adv. Funct. Mater.* **2010**, *20*, 2644–2648.
6. Lee, Y.-D.; Lim, C.-K.; Singh, A.; Koh, J.; Kim, J.; Kwon, I. C.; Kim, S. Dye/Peroxalate Aggregated Nanoparticles with Enhanced and Tunable Chemiluminescence for Biomedical Imaging of Hydrogen Peroxide. *ACS Nano* **2012**, *6*, 6759–6766.
7. Zhang, K.; Kaufman, R. J. From Endoplasmic-Reticulum Stress to the Inflammatory Response. *Nature* **2008**, *454*, 455–462.
8. An, B.-K.; Gierschner, J.; Park, S. Y. π-Conjugated Cyanostilbene Derivatives: A Unique Self-Assembly Motif for Molecular Nanostructures with Enhanced Emission and Transport. *Acc. Chem. Res.* **2012**, *45*, 544–554.
9. Qin, W.; Ding, D.; Liu, J.; Yuan, W. Z.; Hu, Y.; Liu, B.; Tang, B. Z. Biocompatible Nanoparticles with Aggregation-Induced Emission Characteristics as Far-Red/Near-Infrared Fluorescent Bioprobes for *In Vitro* and *In Vivo* Imaging Applications. *Adv. Funct. Mater.* **2012**, *22*, 771–779.
10. Shao, A.; Guo, Z.; Zhu, S.; Zhu, S.; Shi, P.; Tian, H.; Zhu, W. Insight into Aggregation-Induced Emission Characteristics of Red-Emissive Quinoline-Malononitrile by Cell Tracking and Real-Time Trypsin Detection. *Chem. Sci.* **2014**, *5*, 1383–1389.
11. Singh, A.; Lim, C.-K.; Lee, Y.-D.; Maeng, J.-H.; Lee, S.; Koh, J.; Kim, S. Tuning Solid-State Fluorescence to the Near-Infrared: A Combinatorial Approach to Discovering Molecular Nanoprobes for Biomedical Imaging. *ACS Appl. Mater. Interfaces* **2013**, *5*, 8881–8888.
12. Giorgio, M.; Trinei, M.; Migliaccio, E.; Pelicci, P. G. Hydrogen Peroxide: A Metabolic By-Product or a Common Mediator of Ageing Signals? *Nat. Rev. Mol. Cell Biol.* **2007**, *8*, 722–728.
13. Kim, S.; Zheng, Q.; He, G. S.; Bharali, D. J.; Pudavar, H. E.; Baev, A.; Prasad, P. N. Aggregation-Enhanced Fluorescence and Two-Photon Absorption in Nanoaggregates of a 9,10-Bis[4′-(4″-Aminostyryl)styryl]anthracene Derivative. *Adv. Funct. Mater.* **2006**, *16*, 2317–2323.
14. Kim, S.; Pudavar, H. E.; Bonoiu, A.; Prasad, P. N. Aggregation-Enhanced Fluorescence in Organically Modified Silica Nanoparticles: A Novel Approach toward High-Signal-Output Nanoprobes for Two-Photon Fluorescence Bioimaging. *Adv. Mater.* **2007**, *19*, 3791–3795.
15. Kim, S.; Ohulchanskyy, T. Y.; Pudavar, H. E.; Pandey, R. K.; Prasad, P. N. Organically Modified Silica Nanoparticles Co-Encapsulating Photosensitizing Drug and Aggregation-Enhanced Two-Photon Absorbing Fluorescent Dye Aggregates for TPA Two-Photon Photodynamic Therapy. *J. Am. Chem. Soc.* **2007**, *129*, 2669–2675.
16. Jain, R. K.; Stylianopoulos, T. Delivering Nanomedicine to Solid Tumors. *Nat. Rev. Clin. Oncol.* **2010**, *7*, 653–664.
17. Pugh, C. W.; Ratcliffe, P. J. Regulation of Angiogenesis by Hypoxia: Role of the HIF System. *Nat. Med.* **2003**, *9*, 677–684.
18. Moghimi, S. M.; Hunter, A. C.; Murray, J. C. Long-Circulating and Target-Specific Nanoparticles: Theory to Practice. *Pharmacol. Rev.* **2001**, *53*, 283–318.
19. Seo, Y. H.; Cho, M. J.; Cheong, O. J.; Jang, W.-D.; Ohulchanskyy, T. Y.; Lee, S.; Choi, D. H.; Prasad, P. N.; Kim, S. Low-Bandgap Biophotonic Nanoblend: A Platform for Systemic Disease Targeting and Functional Imaging. *Biomaterials* **2015**, *39*, 225–233.
20. Brand, D. D.; Latham, K. A.; Rosloniec, E. F. Collagen-Induced Arthritis. *Nat. Protoc.* **2007**, *2*, 1269–1275.